

## **Towards practical soft X-ray spectromicroscopy of biomaterials**

A. P. HITCHCOCK\*, C. MORIN, Y. M. HENG<sup>+</sup>, R. M. CORNELIUS and J. L. BRASH

*Brockhouse Institute for Materials Research, McMaster University, Hamilton, ON, Canada, L8S 4M1*

Received 21 December 2001; accepted 11 April 2002

**Abstract**—Scanning transmission X-ray microscopy (STXM) is being developed as a new tool to study the surface chemical morphology and biointeractions of candidate biomaterials with emphasis on blood compatible polymers. STXM is a synchrotron based technique which provides quantitative chemical mapping at a spatial resolution of 50 nm. Chemical speciation is provided by the near edge X-ray absorption spectral (NEXAFS) signal. We show that STXM can detect proteins on soft X-ray transparent polymer thin films with monolayer sensitivity. Of great significance is the fact that measurements can be made in situ, i.e. in the presence of an overlayer of the protein solution. The strengths, limitations and future potential of STXM for studies of biomaterials are discussed.

### 1. INTRODUCTION

The adverse effects of implanted biomaterials (regardless of intended anatomic location) begin with the selective interactions of blood proteins with the surface of the biomaterial [1, 2], typically a polymer. In the work reported here, soft X-ray spectromicroscopy is being developed to investigate a number of issues related to selectivity in the first contact of biological systems with polymers which are heterogeneous at the surface through patterning or intrinsic surface or bulk phase segregation. Demonstration of the ability to detect and map adsorbed protein at the monolayer level on surfaces with lateral chemical differentiation is our initial target. Eventually we seek to track site selectivity in the adsorption of specific proteins from mixtures, although this is likely to require labeling techniques since soft X-ray spectroscopy cannot readily distinguish different proteins.

---

\*To whom correspondence should be addressed. E-mail: [aph@mcmaster.ca](mailto:aph@mcmaster.ca)

<sup>+</sup>present address: The Hospital for Sick Children, 555 University Avenue, Toronto, ON Canada M5G 1X8.

Soft X-ray spectromicroscopy (also known as near edge X-ray absorption fine structure or NEXAFS microscopy) is finding increasing use in the analysis of soft materials, on account of its ability to probe chemical complexity quantitatively on spatial scales of 50 nm or better, as well as the versatility with which it can be adapted to a wide range of problems. Reviews of soft X-ray spectromicroscopy techniques, instrumentation, and a broad survey of results have been presented recently [3-6]. Inner-shell excitation or NEXAFS spectroscopy [7] is used as the chemically sensitive image contrast mechanism. For the past few years we have been exploring two techniques of soft X-ray spectromicroscopy for the study of biomaterials and the interaction of biomaterial surfaces with biological subsystems, particularly proteins. Scanning Transmission X-ray Microscopy (STXM) uses a focused X-ray probe with sample scanning and synchronized detection of transmitted X-rays to measure the wavelength dependent optical density through a column of material. Although not intrinsically surface sensitive, it is possible to detect, and thus quantitatively map the distributions of surface species such as proteins if the NEXAFS spectrum of a surface species is sufficiently different from that of the bulk biomaterial constituents. STXM in the water window energy range (200—520 eV) can be applied to samples in vacuum, in air or He at atmospheric pressure, and, of greatest importance to biomaterials, to wet samples enclosed in a cell equipped with X-ray transparent windows.

In this paper we describe only STXM results. We are also engaged in a parallel effort for developing X-ray photoelectron emission microscopy (XPEEM) for biomaterial studies. XPEEM uses large area X-ray illumination (50  $\mu\text{m}$  x 50  $\mu\text{m}$ , at the facility we use) and an electron lens system to record images of the spatial distribution of electrons ejected from a surface following X-ray absorption. Because the electron yield is proportional to the X-ray absorption coefficient, chemical identification and mapping can be derived from the wavelength dependence of the image contrast. The electron lens systems used are most sensitive to the numerous low energy secondary electrons rather than the relatively few primary photoelectrons. Thus the sampling depth is of the order of 5—10 nm, considerably larger than techniques based on energy resolved electron analysis such as X-ray photoelectron spectroscopy (XPS). In addition to chemical sensitivity, XPEEM signals are also very sensitive to topography, local work function variations, and charging, and thus deriving quantitative maps from XPEEM data is much more complicated than with STXM. Finally XPEEM requires a ultrahigh vacuum sample environment, which is not compatible with studies of biomaterials under wet conditions.

## 2. EXPERIMENTAL

### 2.1. X-ray microscopy instrumentation and techniques

Soft X-ray scanning transmission X-ray microscopy (STXM), developed by Kirz, Jacobsen, Ade and co-workers at the National Synchrotron Light Source (NSLS)

[3, 8, 9], is now implemented at several other synchrotron facilities (Advanced Light Source (ALS), Pohang Light Source), and instruments are under construction elsewhere (BESSY, Swiss Light Source (SLS), Canadian Light Source). Panel (a) of Fig. 1 is a sketch of the STXM experiment at the undulator beamline 7.0 at the Advanced Light Source, where this study was performed. The undulator produces high brightness X-rays which are passed through a spherical grating monochromator to select a narrow photon energy range (typically  $\sim 150$  meV). The beam of monochromated soft X-rays is then focused to 50 nm or less by a Fresnel zone plate, then passed through an order sorting aperture to select only the first order diffraction of the zone plate. X-rays transmitted through the sample are detected by conversion to visible light by a fast phosphor, followed by photon detection in single photon counting mode. To obtain an image at a given photon energy, the sample is raster scanned through the focal point while recording the intensity of transmitted X-rays (Fig. 1b). Alternatively, the photon energy can be scanned while sitting at a fixed spot on the sample to acquire the NEXAFS spectra of features of interest (Fig. 1c). The most useful mode is to acquire the NEXAFS signal over a whole field of view, by recording image sequences or stacks [10] (Fig. 1d). Post acquisition analysis of image sequence data is used to correct for image misalignment, and to generate chemical maps, as discussed further below.

Typical incident intensities in the 50 nm focused spot of existing STXMs range from  $10^6$  Hz (NSLS X1A, ALS 5.3.2) to  $10^8$  Hz (ALS 7.0.1) [11, 12]. High brightness third generation light sources are particularly useful to achieve high intensities on the sample and thus rapid scan rates. With sufficient flux, and suitable control and acquisition interfacing, rapid scan rates (currently, 0.2 to 1 ms per pixel at the ALS), and thus high efficiency analytical microscopy, can be achieved. Radiation damage is a concern, but the damage rate relative to the signal acquisition rate is much smaller than in electron microscopy [13]. In these studies we characterize damage rates, we check for extent of damage after key measurements, and we discard data acquired where excessive damage has occurred. STXM is used analytically by acquiring NEXAFS spectra at one location (point mode), along a line (line mode), or through collection of full image sequences (image mode). All of these modes were employed in these studies and are illustrated below.

The transmitted X-ray intensity ( $I$ ) is converted to absorbance (optical density) by using the Beer-Lambert law,  $A = -\ln(I/I_0) = \mu pt = \sigma t$ , where  $I_0$  is the incident flux,  $I$  is the transmitted flux,  $\mu$  is the mass absorption coefficient,  $\rho$  is the density,  $t$  is the thickness and  $\sigma$  is the linear absorption coefficient. The incident flux ( $J_0$ ) is recorded independently with the sample removed (single beam mode of optical spectroscopy). The measured signal averages over a column of the sample and thus it is generally considered 'bulk'-sensitive. However, thin samples (50—200 nm of organic matter at a carbon density of  $\sim 1$  g/cm<sup>3</sup>) are needed to achieve adequate

transmission in the 250—1250 eV soft X-ray range. When the sample is this thin, the surface region (outer ~10 nm) contributes significantly to the transmission mode signal and thus large surface species such as adsorbed proteins can be detected, as illustrated below. In this study, the sample thickness is such that absorption saturation is avoided and there is a linear relationship between absorbance and the thickness-density product.

## 2.2. Data analysis methods

Point spectra, linescan spectra, images, or image sequences are converted to quantitative chemical information (point, line or area compositional maps) by spectral fitting on a pixel-by-pixel basis using linear curve fitting procedures [14-16]. These methodologies, along with many other image and spectral data processing procedures used in this work were accessed by the aXis2000 program [14].

In order to generate quantitative chemical information we fit the spatially resolved NEXAPS signals with reference spectra on a pixel-by-pixel basis. The reference spectra are recorded separately, generally from pure materials. They are placed on absolute linear absorption scales so that the fit coefficient for a given component at a given pixel is the thickness of that component at that position. The ratio of that thickness to the sum of thicknesses of all components fitted is then a measure of the local composition. The array of fitting coefficients for a given component, derived by fitting the individual pixel spectra to linear combinations of reference spectra, is a quantitative chemical *component map*. The fits can be carried out using singular value decomposition [15, 16], linear regression, or a conjugate gradient algorithm. The fit coefficients can be constrained to be positive or they can be treated as freely adjustable parameters. Each methodology provides maps of residuals and a statistical analysis of the errors. Comparison of the results from different algorithms helps build confidence in the significance of weak signals such as those associated with proteins on polymer surfaces. Where vertical scales are provided for the component maps in the figures shown below, these indicate the estimated thickness in nm of that component, if it was pure. Typically a given pixel can have contributions from 3 or more components. Estimated uncertainties are 10 - 15%. Systematic errors are considerably larger than statistical errors (the latter are typically 1 - 3% for the majority components). The uncertainty in the quantitation of the weak signal from surface adsorbed proteins is considerably higher — perhaps as much as 50%. In addition to grayscale maps of individual components, we present color maps where the intensity of the red, green or blue component gives the spatial distribution of that component over the region mapped. In all color maps presented here we have individually byte-scaled each component and thus the intensity of one component relative to the other is not properly represented. This approach provides clearer information of spatial localization of the components, since it makes the weak protein signals visible against the much stronger polymer components. With byte-rescaling one must be careful in interpreting intermediate colors, although they do indicate regions where multiple components are present in the column sampled.

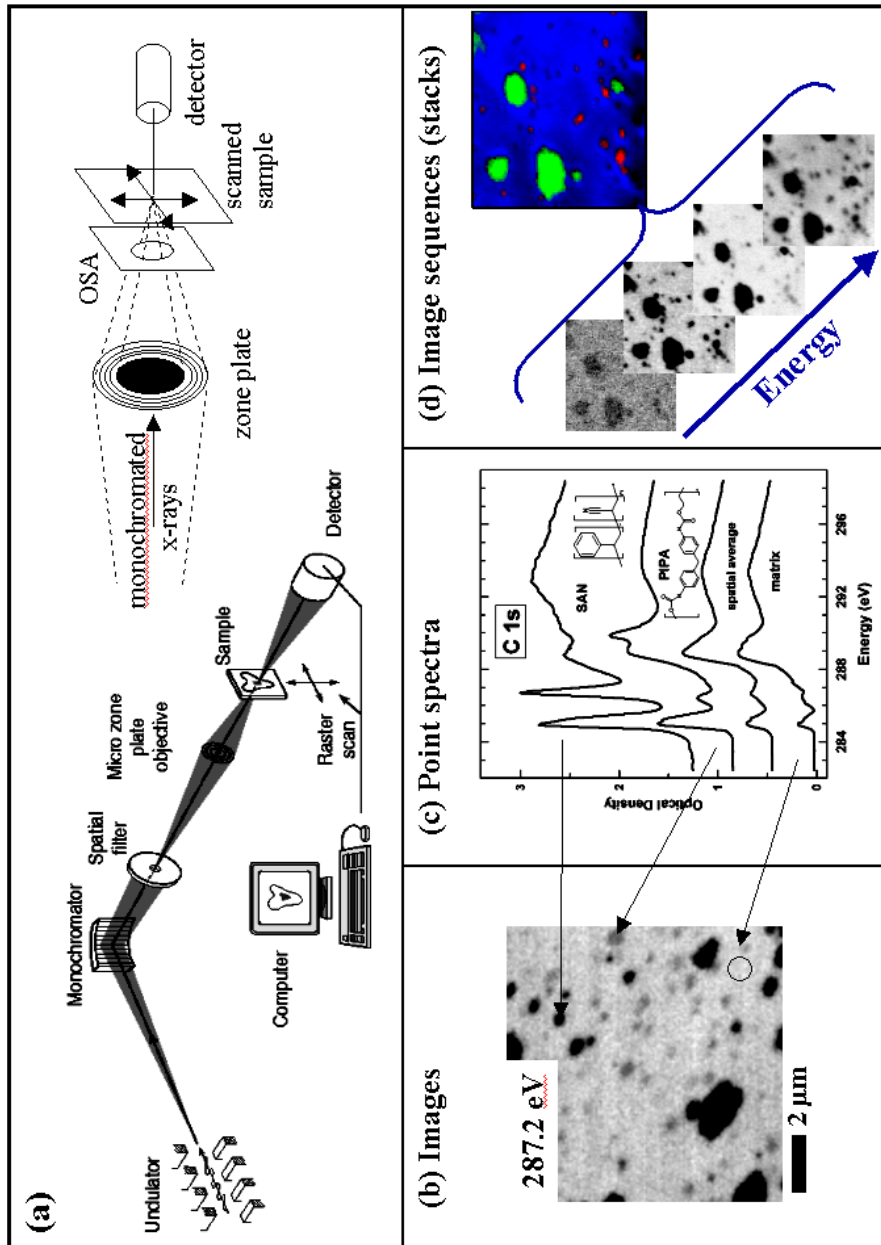


**Figure 1.** (a) Schematic of undulator beamline 7.0 and the STXM endstation at the Advanced Light Source (ALS) BL 7.0. The inset shows details of the STXM optics. (b) Image of sample #355, a compressed polyurethane foam with styrene acrylonitrile (SAN) and poly-isocyanate poly-addition product (PIPA) filler particles. This image was recorded at 287.2 eV, the energy of the C  $\rightarrow$   $\pi^*$  CN transition at which the SAN particles selectively absorb. (c) Spectra from spatially selected regions compared to a defocused sample average spectrum. These spectra were actually obtained from an image sequence, but equivalent point spectra can be acquired with the STXM. (d) Illustration of the image sequence (stack) concept. Four of 120 images are displayed, along with a color coded chemical constituent map derived by pixel-by-pixel curve fitting (R = PIPA, G = SAN, B = matrix).

### 2.3. Substrates and protein exposure methods

#### 2.3.1. Materials.

2.3.1.1. *Substrates.* Three different substrates were used, all provided by Dow Chemical. All three consist of a compressed polyurethane foam, with a TDI (toluene diisocyanate) hard segment and a butane oxide (BO) soft segment. The three differ with regard to types of filler particles. One substrate (code #355) contains poly(styrenecoacrylonitrile (SAN) and poly-isocyanate poly-addition product (PIPA, a methylene diphenyl diisocyanate (MDI)-based hard segment-like material), both referred to as copolymer polyol (CPP) filler particles. The second substrate (code #530) contains only SAN particles. The third substrate (code #529) contains only PIPA particles. The synthesized foams were cryo microtomed to 100 nm thickness and multiple sections were placed either on TEM grids or on 4-pane Si<sub>3</sub>N<sub>4</sub> windows (2 x 2 array 1.25 x 1.25 mm membrane, 75 nm thick; frame size is 7.5 mm x 7.5 mm, 200 µm thick Si). The silicon nitride (Si<sub>3</sub>N<sub>4</sub>) windows were obtained from Silson Ltd. [17] and were rigorously cleaned to semiconductor industry standards by the manufacturer. They were removed from plastic storage capsules and used without further surface preparation.

2.3.1.2. *Deionized water.* From Sigma, HPLC water, residue after evaporation <0.0003%.

2.3.1.3. *Protein.* Human serum albumin (HSA) was from Behringwerke AG, Marburg, Germany, and is reported to be homogeneous as judged by sodium dodecyl sulphate polyacrylamide gel electrophoresis (SDS-PAGE). Fibrinogen (Fg) was from Calbiochem, San Diego, California, USA. It is prepared from human plasma and is plasminogen depleted. It is reported to be >95% clottable by thrombin, and is homogeneous as judged by SDS-PAGE.

2.3.1.4. *Buffers.* The phosphate buffer saline packs were from Pierce, Rockford, IL, USA.

2.3.2. *Sample preparation and mounting methods.* Dry sections of the polyurethanes (#355, #529 or #530) deposited on a TEM grid were exposed for 20 min to 1 ml of 0.1 mg/ml protein solution (albumin or fibrinogen) in deionized H<sub>2</sub>O or phosphate buffer. For the sample in Fig. 3, the droplet of solution was allowed to dry out on the surface, thus depositing 0.1 mg over perhaps 0.5 mm<sup>2</sup>. This corresponds to an average thickness of 200 nm (assuming  $\rho = 1 \text{ g/cm}^3$ ) For the sample in Fig. 4, a 5 µl drop of 0.1 mg/ml Fg in saline phosphate buffer was deposited over a #355 section (deposited on a Si<sub>3</sub>N<sub>4</sub> window). Such a drop covers an area greater than that of the section itself. At the end of the 20 minute exposure time, the drop had not evaporated. Three consecutive rinses of the remaining drop were done by sucking in and out the drop with 50 µl volumes of deionized water. The sample was then loaded into the STXM. For the sample in Fig. 5 a #355 section was exposed

to fibrinogen as above. It was then extensively washed to remove excess protein, dried and then rehydrated by adding a drop of water on top of the section. A second window was then placed on top of the first one, thereby creating a water layer over the section between the two windows.

For the samples in Figs 6 and 7, a 5  $\mu$ l drop of 0.01 mg/ml Fg in freshly prepared phosphate buffer was deposited over a #355 section on a Si<sub>3</sub>N<sub>4</sub> window. A second window was immediately placed over it and the sample was placed in the STXM about 10 min after fabrication. Due to instrumental difficulties, the sample was not measured until 2 h after fabrication.

### 3. RESULTS

#### 3.1. STXM of CPP containing polyurethanes: substrate characterization

The polyurethane substrates used in this study were supplied by Dow Chemical as cryo-microtomed thin sections placed on TEM grids or silicon nitride windows. They consist of a polyurethane matrix with a TDI hard segment and a butane oxide soft segment, in which one or more types of copolymer polyol (CPP) particles are embedded [18]. These CPP particles provide chemically differentiated domains at the surface with sizes in the 0.1 to 2 micron range, which is well suited to the spatial resolution of current X-ray microscopes. In contrast the ‘natural’ phase segregation in most polyurethanes is at a 10 - 30 nm scale [18] which is too small for current X-ray microscopy capabilities. Both particle materials — SAN and PIPA — are aromatic and hydrophobic in character, while the matrix of the polyurethane is an aliphatic polyether which is more hydrophilic.

In other studies we have shown that C 1s NEXAFS spectroscopy can readily distinguish the urea and urethane linkages present in polyurethanes; determine polyol content; and identify the types of R and R’ groups in a given polyurethane [19-21]. NEXAFS signals in STXM have been used to map key functional groups quantitatively — urea, urethane and polyol in native polyurethanes [22], and the types of filler particles [6, 23]. STXM spectromicroscopy is being used to help understand how filler materials affect mechanical properties such as elastic modulus, tear strength and resiliency, and to aid the development of improved fillers [23].

Figure 1 shows the spectral signatures of the SAN, PIPA and polyurethane matrix, and their spatial distributions in the (#355) substrate. The #530 SAN polyurethane substrate was similar except it did not have any of the small PIPA particles and the SAN particles were somewhat larger than in #355. The #529 polyurethane substrate has only PIPA particles and again, the particle size distribution includes larger PIPA particles than found in #355.

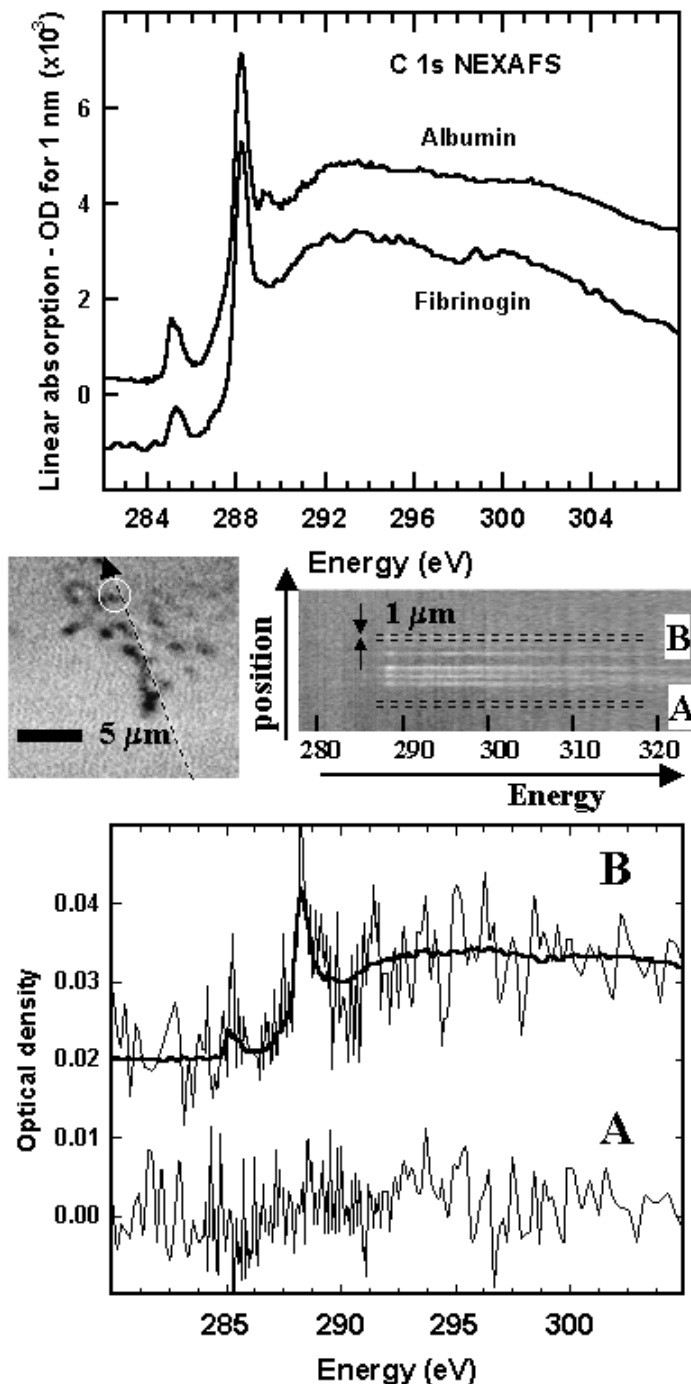


**Figure 2.** (top) Comparison of the C 1s NEXAFS spectra of albumin and fibrinogen recorded in the STXM. (lower) Illustration of monolayer sensitivity of STXM spectroscopy to pure albumin. The central panel displays an image (288.2 eV) of a deposit of pure albumin on a silicon nitride window (dry), and the signal from a linescan spectrum across the dotted line. The spectra shown in the lower panel were extracted from the linescan by adding signal over less than 1 micron in the areas indicated by dashed lines, labeled A and B. Spectrum B is offset vertically by 0.02 units. The OD of only 0.01 in the C 1s continuum is equivalent to 3 nm protein. An albumin molecule in its standard conformation is 3 x 8 nm, indicating monolayer sensitivity.

### 3.2. Protein-polymer interaction studies

Eventually we intend to apply our technique to studies of protein decorated polymer samples while they are fully covered with a solution layer that has a composition of that of the relevant biological system, such as blood plasma. At present we are exploring STXM studies of both dry and wet samples to understand and optimize our data acquisition and analysis methods. Results to date indicate that while STXM is essentially a ‘bulk’ technique, protein monolayer detection is possible, although close to the current limit of sensitivity [6]. In particular, the sensitivity to an adsorbed layer depends on how different the adsorbate spectrum is relative to that of the underlying substrate. We find the most reliable detection of weak protein deposits when we use the full spectral signature in analysis of a full image sequence (40–80 energies) rather than simply imaging at one or a few photon energies.

The upper panel of Fig. 2 presents the C 1s spectra of albumin and fibrinogen. The spectra are rather similar, with each being dominated by the strong peak at 288.2 eV, which is the C 1s(C=O)  $\rightarrow$   $\pi^*_{\text{C=O}}$  transition at the amide group of the peptide bond. Each also shows a weak peak at 285.1 eV, associated with C 1s(C=C)  $\rightarrow$   $\pi^*_{\text{C=C}}$  transitions at the phenyl groups of aromatic amino acids. One small difference between the spectra of albumin and fibrinogen is that albumin has a weak peak at 289 eV which is not seen in fibrinogen. Since each protein has some of each of the 20 amino acids, it is expected that averaging over such distributions leads to very little differentiation. This is in sharp contrast to the isolated amino acids where it is straightforward to identify the amino acid from the C 1s spectrum [24].

The lower section of Fig. 2 explores the STXM detection limits for pure protein in the absence of any other organic material. The deposit of albumin from a very dilute solution on a clean silicon nitride window shows a readily differentiated C 1s spectrum typical of protein which is three to four times more intense than the noise in a blank (the spectrum from an equivalent length of the adjacent window which does not have deposited protein). The optical density associated with the protein signal in the circled region is equivalent to a sample thickness of 3 nm, approximately the expected thickness of an albumin monolayer.

Figure 3 reports the result of a measurement of a sample consisting of human serum albumin deposited onto the #529 PIPA polyurethane substrate. This sample was prepared by placing a drop of a 1 mg/ml solution onto the microtomed section supported on a 3 mm TEM grid. An uneven distribution of the albumin was left on the surface after solvent evaporation. A region at the edge of a thick deposit was chosen to explore the detection sensitivity. The strength of the protein-like C 1s NEXAFS signal, in the regions where the map indicates the weakest signal which can be attributed to protein (circle in Fig. 3), is approximately equivalent to a monolayer. This sample was not prepared as a controlled biomaterial — protein interaction but it is of historical interest since it was our first demonstration of the surface sensitivity of STXM and thus the viability of the technique.

Figures 4–7 show results from mapping fibrinogen (Fg) adsorbed on a microtomed section of the 2-filler #355 polyurethane system presented in Fig. 1. These

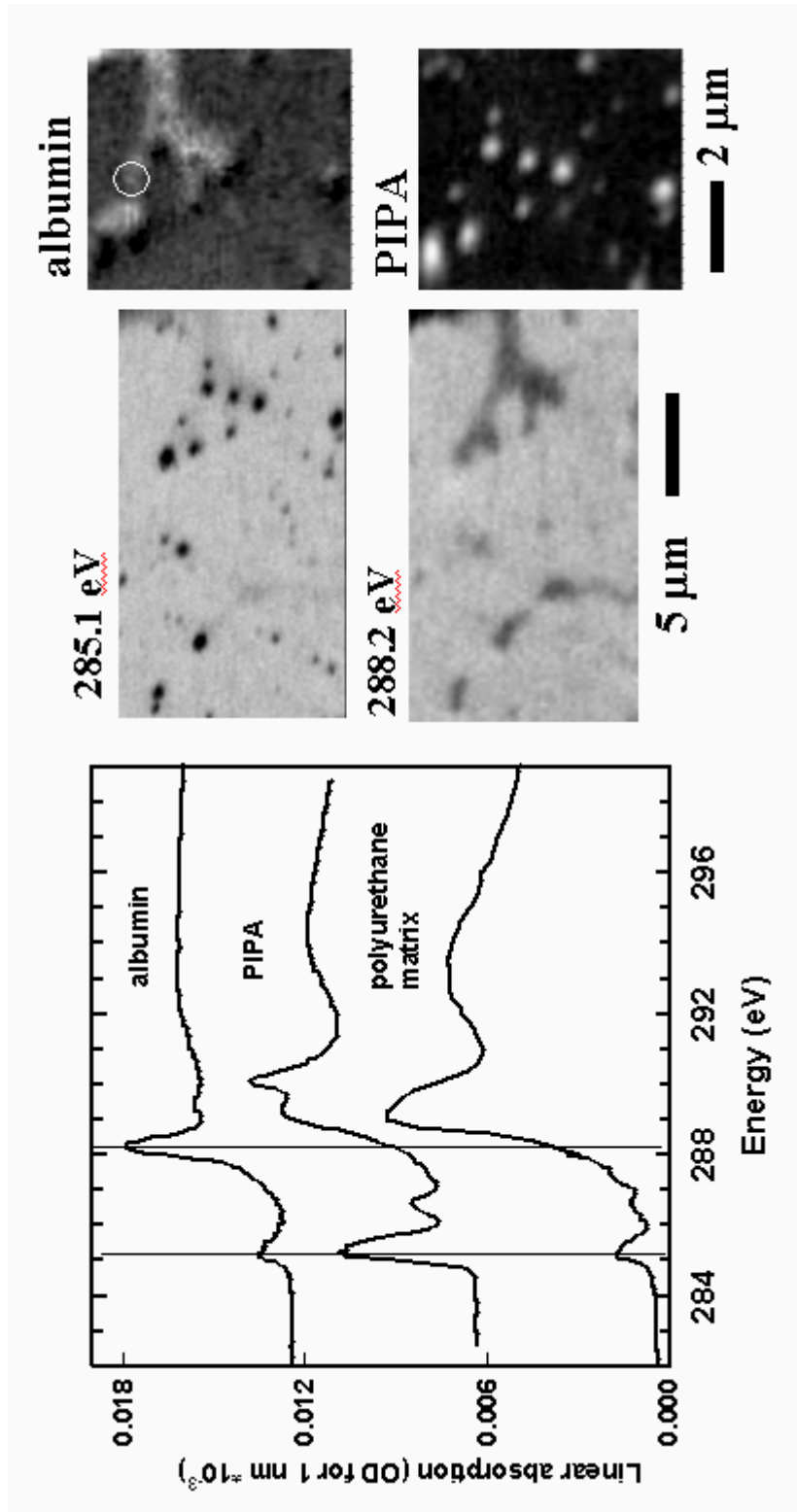


**Figure 3** Reference spectroscopy (left), transmission images at 285.1 eV (highlighting PIPA) and 288.2 eV (highlighting protein) (center); and (right) component maps of albumin and PIPA derived from a C 1s image sequence recorded from a thin section sample of #529 (PIPA-in-TDI polyurethane) with deposited albumin, measured in the dry state. In the weakest regions of the albumin 'smear' (e.g. the circled region), the signal is at the monolayer level.

figures exemplify four different steps in the evolution of our ability to detect proteins on polymer surfaces. For the sample shown in Fig. 4, the fibrinogen was adsorbed on the sample by immersion for 20 min in a dilute solution (0.1 mg/ml) in buffer. Excess protein solution was removed by thorough rinsing without taking the sample through the air-water interface. The sample was then dried. The microtomed sample has three classes of chemical constituents exposed at the surface — polyether-rich matrix, SAN and PIPA. The left part of Fig. 4 plots the reference spectra used in the data analysis. The labeled component maps indicate the spatial distribution of the identified components. The residual shows a map of the difference between the fit and the actual image sequence, integrated over the full energy range (54 energies between 282 and 292 eV). The residual map represents deviations between the fit and the measured signal of less than 5%. The spatial distribution of the residuals indicates that the SAN reference spectrum is not a perfect match to the SAN in this sample. While there is some misidentification in these maps associated with limitations of the reference spectra and statistical noise, the high signals in the Fg map indicate positions of preferred adsorption on the surface. The registry of the protein relative to the other components is indicated in the final part of Fig. 4 namely the color-coded composite component map in the lower right part. Here the individual SAN, PIPA and protein maps have been combined by assigning red to SAN, green to PIPA and blue to fibrinogen. The intensities within each color have been byte scaled, so that the very weak protein signal can be located relative to the strong SAN and PIPA signals. In this preparation, we find that fibrinogen has a preference to be attached to the matrix beside the SAN particles, with also indication from the orange color of some adsorption on top of the SAN particles.

The sample examined in Fig. 5 was prepared as that for Fig. 4 but, just prior to STXM analysis it was rehydrated with a small drop of deionized water then capped by a second silicon nitride window to form a wet cell. In this measurement we wished to explore the ability of STXM to detect protein adsorbed on a polymer in an environment of reduced contrast caused by the X-ray absorption of an aqueous overlayer of a few micrometers in thickness. The results indicate that STXM can detect adsorbed proteins on polymers in the presence of thin aqueous overlayers. Furthermore the amount of fibrinogen detected is in the monolayer range in some regions. In addition to the color-coded composite component map, Fig. 5 shows a fit to the C 1s NEXAFS spectrum extracted from pixels which have high fibrinogen content. These pixels were identified by generating a binary mask based on an intensity threshold for the fibrinogen map (threshold set to 60 nm), and using that mask to define the region of interest for spectral extraction from the full image sequence. The spectrum in the high-Fg region is primarily that of the matrix rather than SAN. We have compared this analysis to that of the adjacent SAN particles (not shown). The quality of the fit is equally good. The amount of Fg determined on top of the SAN particles is only 10 nm, a signal level similar to the residual of the fit.

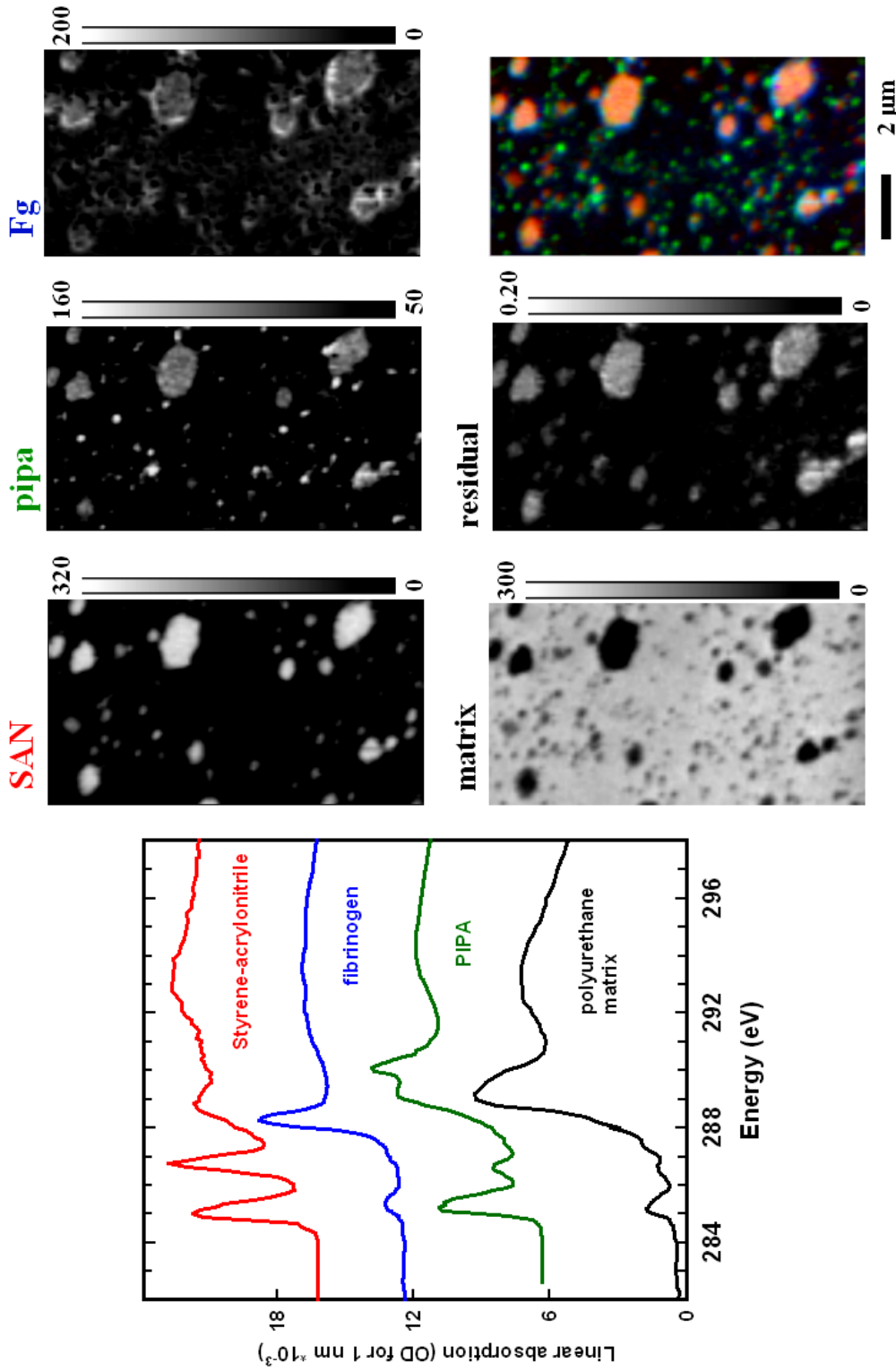


**Figure 4** Analysis of STXM of fibrinogen adsorbed on #355 (TDI) polyurethane with PIPA and SAN filler particles) measured in the dry state. The sample was prepared by a true adsorption process from buffer at low concentration (0.1 mg/ml) followed by carefully washing off the excess protein then drying. (left) reference spectra, placed on absolute linear absorption scales. Four of the six ‘image’ panels are the quantitative component maps of the SAN, PIPA, fibrinogen and matrix components; the vertical gray scale of each is the approximate thickness of that component in nm. The other two are the map of the residuals averaged over the full energy range measured and a color coded component map (red = SAN, green = PIPA, blue = Fg).

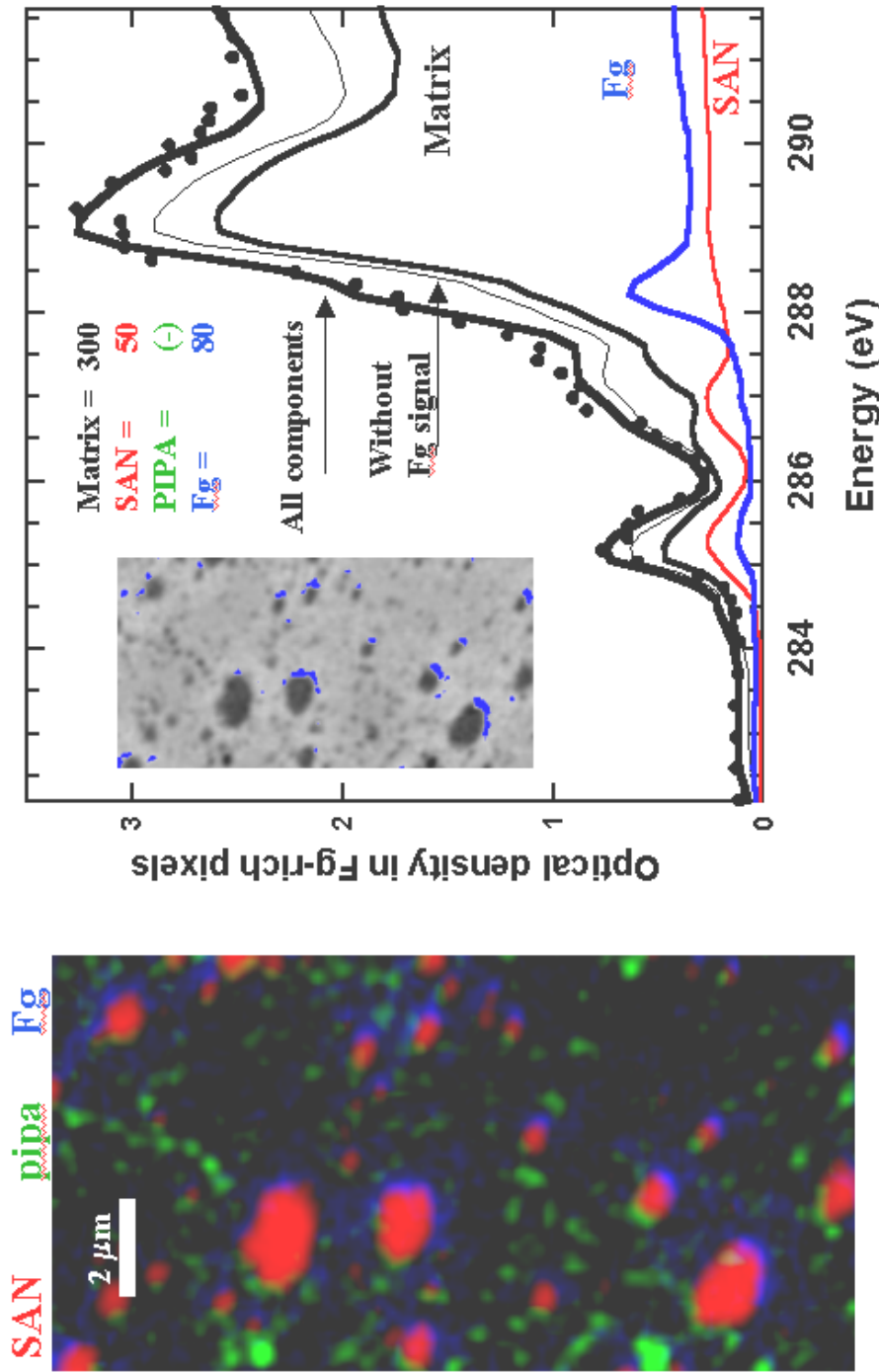


**Figure 5** (left) Color-coded composite image derived from a C 1s STXM image sequence of fibrinogen adsorbed from a 0.1 mg/ml buffer solution onto #355 substrate. The measurements were made with the sample rehydrated by a  $\sim 1 \mu\text{m}$  thick layer of deionized water in a silicon nitride wet cell, in order to explore the masking effect of overlaid water. The combined byte-scaled SAN (red), PIPA (green) and protein (blue) component maps displays the spatial relationship of the protein relative to the two types of filler particles and the matrix. (right) Spectrum of the blue highlighted regions in the insert image (pixels where the Fg signal indicates more than 60 nm) along with decomposition into the four fitted components. The points are data, the thickest solid line the fit with all components, the thinnest line the fit without fibrinogen, and the other lines the individual components.

These results indicate that fibrinogen has a strong preference to adsorb at the edges of the SAN particles but still to be attached to polyurethane matrix rather than SAN. Similarly, on the #530 substrate the albumin is seen to adsorb preferentially at the edges of the PIPA particles (see Fig. 3). Several factors might explain this preference. First there could be special aspects of this substrate at the interface of the CPP particles and the polyurethane matrix that enhance bonding to proteins. Second, adsorption at edges of harder, aromatic filler particles could reflect 'mechanical trapping'. The SAN particles protrude significantly from the matrix as much as 50 nm based on the total sample thickness derived in the analysis. A simple, perhaps overly naïve, model of such trapping would be entanglement of protein molecules (possibly partially denaturing in the process) on the protruding filler particles. A more sophisticated mechanism could be entropically driven deposition [25] in which the protein in solution would be considered to play a role. At this point it is not possible to define the mechanism of preferential attachment, simply to note there is a clear preference for fibrinogen to adsorb on the matrix side of the boundary of the CPP particles (particularly SAN) and the polyurethane matrix, and that the STXM technique is capable of detecting that fibrinogen in a quantitative manner.

Figure 6 presents the color coded component map derived from a C 1s image sequence measured from a filler-polyurethane sample (#355) with an overlayer of solution containing 0.01 mg/ml fibrinogen in buffer. In this presentation the (R = SAN, G = PIPA, B fibrinogen) map has been superimposed on the gray scale map of the polyurethane matrix component. This is essentially the type of 'in situ' system which is the experiment of ultimate interest, since the solution overlayer contains both buffer salts and protein. These additional solution components might be expected to reduce the contrast of the adsorbed protein relative to the other components. At first we were concerned that the C 1s signal of the protein in the solution could mask the adsorbed protein. Relative to monolayer surface levels, the amount of protein present in a 10  $\mu\text{m}$  high, 1  $\mu\text{m}$  diameter column of a 0.01 mg/ml fibrinogen solution is about the same as that adsorbed at a monolayer coverage on a 1  $\mu\text{m}$  diameter circle of a surface. Thus one might expect a background signal from the free protein over the whole surface, which could mask detection of surface adsorption sites. However, this background signal has not been detected. We speculate that local heating of the solution from the X-ray beam could induce increased thermal motion which might tend to move protein in the solution away from the impinging beam. Experiments to seek the threshold for interference from solution protein will be performed. So far, these results indicate that it is possible to map protein on surfaces from 0.01 mg/ml and even considerably more concentrated solutions since we have measured surface adsorbed protein with protein solution overlayers of up to 0.1 mg/ml concentration.

Figure 7 shows the same Fg/#355 sample investigated at the N 1s edge. This figure plots the N 1s reference spectra of the matrix, PIPA, SAN and fibrinogen, along with the color coded composite map of the SAN, PIPA and fibrinogen

components. The N 1s edge is particularly favorable for studies of protein relative to polymer substrates since proteins have a strong N 1s  $\rightarrow \pi^*_{\text{amide}}$  transition at 402 eV, [26] whereas many polymers do not contain unsaturated N environments. The SAN also has a strong N 1s  $\rightarrow \pi^*_{\text{CN}}$  transition at 399.8 eV which is readily distinguishable from the higher energy protein signal. However the PIPA and matrix have very similar N 1s signals and thus the PIPA component is less well detected than at the C 1s edge. The quantitative chemical analysis at the N 1s edge gives similar results to that at the C 1s edge (note that the areas measured for Figs 6 and 7 are different). The interesting aspects of the results shown in Figs 6 and 7 are: (1) There was no interference from the protein or buffer salts present in the overlayer solution. (2) The mapping of the fibrinogen derived from the C 1s and N 1s edges is very similar, indicating that detection is not an artifact of a mismatch of model spectra and the unknown. (3) The location of the protein is consistently at the sides of the SAN particles but on the matrix, not on the SAN, in all studies of the protein exposed sample #355.

Together these results constitute clear evidence that STXM can detect proteins at polymer surfaces under aqueous layers containing inorganic buffer salts and protein. We do note that the quantitative accuracy is limited and that the enclosed results may be affected to some degree by residual misalignment. In the as-recorded image sequences there are drifts as large as a few microns in the field of view associated with poor tracking of the zone plate along the X-ray axis (it is necessary to move the ZP with photon energy to maintain focus). Software procedures [10, 14] remove most of this misalignment but there is residual jitter of as much as a hundred nanometers. Recently we have measured the dry Fg/#355 system using a new STXM at the ALS, one which uses a two dimensional interferometer system [12] to maintain a constant field of view. The results were very similar to those presented here.

#### 4. DISCUSSION AND SUMMARY

These results demonstrate that STXM is a viable technique to address questions of chemical differentiation of substrates and protein localization at the surfaces of biomaterials under conditions which are relatively close to their actual use. This is in distinct contrast to vacuum based techniques such as TOF-SIMS, XPS or XPEEM where there is always a question whether the absence of water or buffer changes the character of the interface, e.g. by inducing surface segregation of hydrophobic components. STXM provides information on lateral morphology for both dry and wet samples. This is potentially useful for studying artificially patterned biomaterials, chemical mapping of biomaterial substrates, and quantitative mapping of adsorbed protein relative to the substrate. Perhaps the weakest aspect of the STXM method is the lack of intrinsic depth resolution since the signal at any location is a column average. It is very unlikely that the protein signal arises from anywhere but the polymer surface. However the same cannot be said for the signal from the underlying polymer. In that respect XPEEM should be a

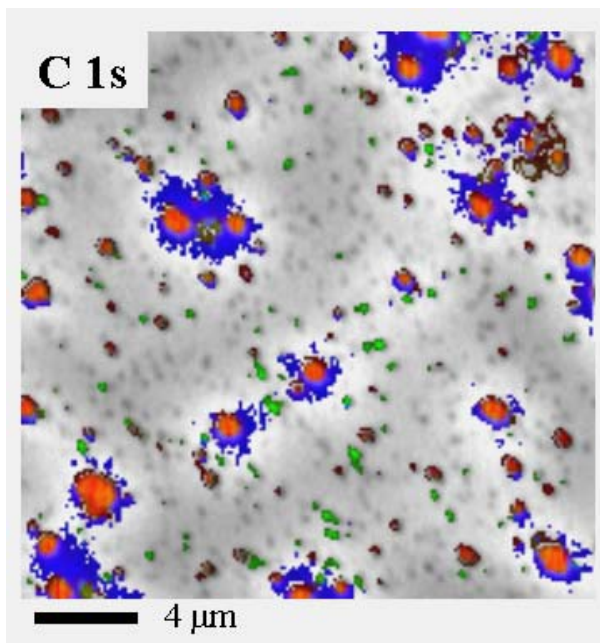


**Figure 6.** Color-coded composite image derived from a C 1s STXM image sequence of a #355 sample covered with a protein solution (fibrinogen in buffer, 0.01 mg/ml). In this case a byte-scaled combination of the SAN (red), PIPA (green) and protein (blue) component maps has been superimposed on a gray scale image of the polyurethane matrix map. This result was derived from an image sequence measurement of a sample with the fibrinogen buffer solution left over the surface. The overlayer of buffer is estimated from the pre-edge signal to be ~5 microns thick.

useful complement to STXM since it has the potential to provide better surface characterization of polymer substrates at similar spatial resolution. Indeed recently we have made a detailed AFM — STXM — XPEEM comparison of the surfaces of polystyrene— polymethylmethacrylate blends [27] which showed very considerable differences between composition and morphology of the bulk as sampled by STXM, and that of the surface as sampled by XPEEM. The XPEEM and AFM images showed similar morphology, but the conventional interpretation of the AFM based on comparing bulk sample composition with relative areas of the continuous and discontinuous domains, was found to give an inverted assignment of the chemical identity of the domains. On the other hand the much higher spatial resolution of the AFM revealed micro-domain features which were not detected by XPEEM, and were just barely detectable by STXM. As in many other fields, the most effective way to solve complex problems such as biomaterial interfaces is to use multiple techniques with proper recognition of the strengths and weaknesses of each technique. This philosophy has been a hallmark of the scientific career of Dr. Brash, to whom this article is dedicated.

Dramatic improvements are currently underway in scanning transmission X-ray microscopy instrumentation, performance and analysis methodology. Cryo-STXM has been implemented recently at NSLS [28]. Two microscopes with interferometric

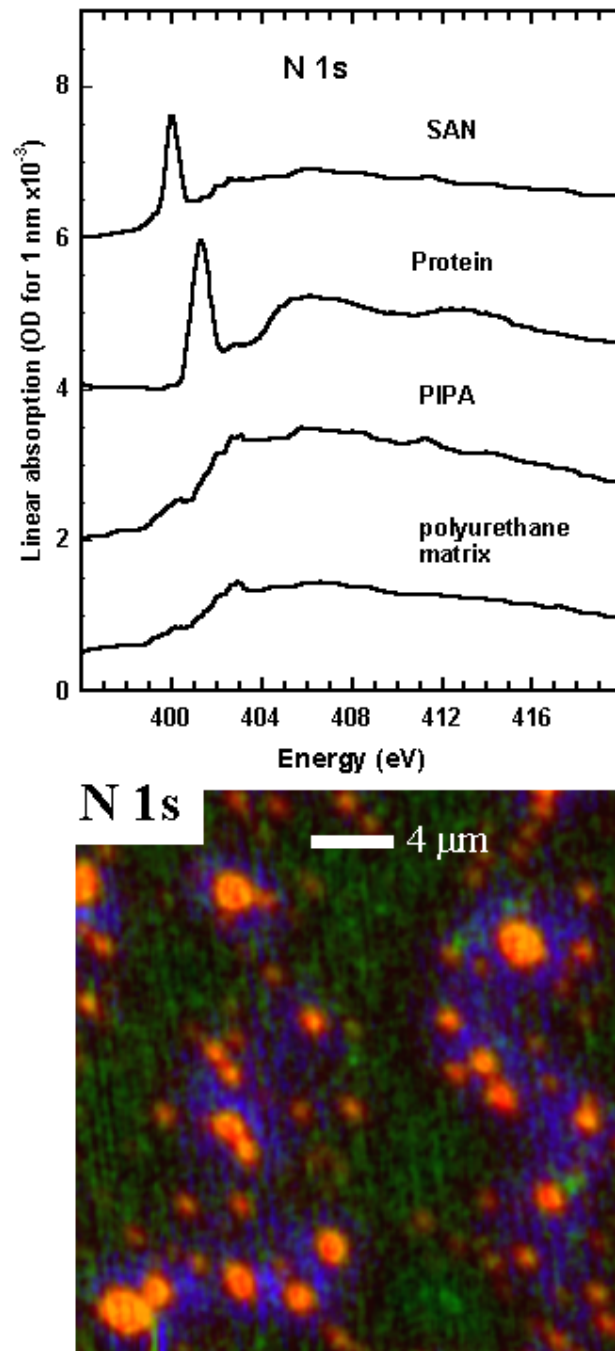


**Figure 7.** Color-coded composite image derived from a N 1s STXM image sequence of fibrinogen adsorbed from a 0.01 mg/ml buffer solution onto #355 substrate. This is a different area of the same sample for which the C 1s results are plotted in Fig. 6. The N 1s spectra of the pure reference materials are also plotted. The protein spectrum is from albumin recorded at a different synchrotron facility [26], while the N 1s spectra of SAN, PIPA and the matrix were those of the pure #355 material [23].

control of sample-zone plate position have recently been commissioned at the ALS [11]. The interferometric signal provides a precise solution to a major problem in earlier instruments, namely drift in the field of view as the photon energy is scanned. These new instruments will allow detailed studies of many biomaterials problems. In a few years it will be possible to readily carry out orientation contrast studies. Early studies [29] showed that orientation contrast can be an important aspect of polymer X-ray microscopy. However those measurements were extremely tedious since the sample had to be removed, rotated, and the same region found in the new orientation. In a few years time there will be STXM microscopes on beam lines at the ALS, Swiss Light Source, and the Canadian Light Source, which will be illuminated by elliptically polarized undulators (EPU). When proper control of the phase shifting of the separate sections is employed, EPUs can produce linearly polarized light with user selectable, arbitrary orientation [30]. This will allow routine exploitation of polarization contrast which will be important for studying polymeric biomaterials with aligned molecules. Finally, a significant portion of the polymer and biomaterial soft X-ray microscopy research carried out to date has been performed by, or in collaboration with industrial researchers. The rapid recognition by industry of the remarkable value of soft X-ray microscopy techniques attests to the added value NEXAFS microscopy brings to practical problem solving relative to other, more accessible, lab-based analytical microscopy techniques. It may be anticipated that the biomaterials industry will recognize the benefits of STXM for investigating and thus advancing their materials.

### *Acknowledgements*

This work is funded by the Natural Science and Engineering Research Council (Canada) and the Canada Research Chair program. The ALS STXM was developed by T. Warwick (ALS), B. P. Tonner (U Wisconsin Milwaukee) and collaborators, with support from the US DOE under contract DE-ACO3-76SF00098. Zone plates used at the ALS were provided by Eric Anderson of CXRO, LBNL. We thank ALS staff for much assistance and expert operation. We thank especially Ed Rightor, Werner Lidy and Gary Mitchell (Dow Chemical) for providing the polyurethane substrates, and Rick Steele, George Meigs, Eli Rotenberg and Tony Warwick (Advanced Light Source, Berkeley) for their capable work in developing and maintaining the ALS 7.0 beamline and STXM.

### **REFERENCES**

1. R.M. Cornelius and J. L. Brash, *Biomaterials*, **20**, 341 (1999).
2. A.M. Botelho do Rego, O. Pellegrino, J.M.G. Martinho and J. Lopes da Silva, *Langmuir* **16**, 2385 (2000).
3. J. Kirz, C. Jacobsen and M. Howells, *Q. Rev. Biophys.*, **28**, 33, (1995).
4. H. Ade, in *Experimental Methods In The Physical Sciences*, **32**, J.A.R. Samson and D.L. Ederer Ed., Vol. 32, p. 225. Academic Press (1998)
5. H. Ade and S.G. Urquhart, in “*Chemical Applications of Synchrotron Radiation*” T. K. Sham, ed. World Scientific Publishing (2002)
6. A.P. Hitchcock, *J. Synchrotron Radiation* **8**, 66 (2001)
7. J. Stöhr, *NEXAFS Spectroscopy*, Springer Tracts in Surface Science **25** (1992).
8. H. Ade, X. Zhang, S. Cameron, C. Costello, J. Kirz and S. Williams, *Science* **258**, 971 (1992).

9. H. Chapman, C. Jacobsen and S. Williams, *Ultramicroscopy* **62**, 191 (1996).
10. C. Jacobsen, S. Wirick, G. Flynn and C. Zimba, *J. Microscopy* **197**, 173 (2000).
11. T. Warwick, H. Ade, D. Kilcoyne, M. Kraitsch, T. Tyliczszak, S. Fakra, A. P. Hitchcock and H. Padmore, *J. Synchrotron Rad.* **9**, 254 (2002).
12. A.L.D. Kilcoyne, T. Tyliczszak, R. Steele, A.Peter Hitchcock, S. Fakra, K. Frank, C. Zimba, E. Rightor, G. Mitchell, I. Koprinarov, E. Anderson, B. Harteneck, Adam. P. Hitchcock, T. Warwick, H. Ade, *J. Synchrotron Rad.* (2002) in press..
13. E.G. Rightor, A.P. Hitchcock, H. Ade, R.D. Leapman, S.G. Urquhart, A.P. Smith, G. Mitchell, D. Fischer, H.J. Shin and T. Warwick, *J. Phys. Chem. B* **101**, 1950 (1997).
14. aXis2000 is an IDL 'widget' (application), which is available from <http://unicorn.mcmaster.ca/aXis2000.html>. IDL is a Kodak company – www.rsinc.com
15. X. Zhang, R. Balhorn, J. Mazrimas and J Kirz; *J. Struc. Biol.* **116**, 335 (1996).
16. I. Koprinarov, A.P. Hitchcock, C.T. McCrory and R.F. Childs, *J. Phys. Chem. B* **106**, 5358 (2002).
17. Silson Ltd. JBJ Business Park, Northampton Road, Blisworth, Northampton England, NN7 3DW
18. R. Herrington, *Flexible Polyurethane Foams*, 2 ed., The DOW Chemical Company (1997).
19. S.G. Urquhart, A.P. Hitchcock, R.D. Leapman, R.D. Priester and E.G. Rightor, *J. Polymer Science B: Polymer Physics*, **33**, 1593 (1995).
20. S.G. Urquhart, H. Ade, A.P. Smith, A.P. Hitchcock, E.G. Rightor and W. Lidy, *J. Physical Chemistry B* **103**, 4603 (1999).
21. S.G. Urquhart, A.P. Hitchcock, A.P. Smith, H. Ade, W. Lidy, E.G. Rightor and G.E. Mitchell, *J. Electron Spectrosc.* **100**, 119 (1999).
22. E.G. Rightor, G.E. Mitchell, S.G. Urquhart, A.P. Smith, H. Ade, A.P. Hitchcock, A. Aneja and R.J. Wilkes, *Macromolecules* **35**, 5873 (2002).
23. A.P. Hitchcock, I. Koprinarov, T. Tyliczszak, E.G. Rightor, G.E. Mitchell, M.T. Dineen, F. Hayes, W. Lidy, R.D. Priester, S.G. Urquhart, A.P. Smith, H. Ade, *Ultramicroscopy* **88**, 33 (2001).
24. K. Kaznachev, A. Osanna, C. Jacobsen, O. Plashkevych, O. Vahtras, H. Ågren, V. Carravetta and A.P. Hitchcock, *J. Phys. Chem. B* **106**, 3153 (2002)
25. K.H. Lin, J.C. Crocker, V. Prasad, A. Schofield, D.A. Weitz, T.C. Lubensky and A.G. Yodh, *Phys Rev Lett.* **85**, 1770 (2000).
26. B.W. Loo, Jr., I.M. Sauerwald, A.P. Hitchcock and S.S. Rothman, *J. Microscopy* **204**, 69 (2001).
27. C. Morin, H. Ikeura-Sekiguchi, T. Tyliczszak, R. Cornelius, J.L. Brash, A.P. Hitchcock A. Scholl, F. Nolting, G. Appel, A. D. Winesett, K. Kaznachev and H. Ade, *J. Electron Spectroscopy* **121**, 203 (2001).
28. J. Maser, A. Osanna, Y. Wang, C. Jacobsen, J. Kirz, S. Spector, B. Winn, and D. Tennant, *J. Microscopy*, **197**, 68 (2000).
29. A.P. Smith and H. Ade, *Appl. Phys. Lett.* **69**, 3833 (1996).
30. A.T. Young, E. Arenholz, S. Marks, R. Schlueter, C. Steier, H. A. Padmore, A.P. Hitchcock and D.G. Castner, *J. Synchrotron Rad.* **9**, 270 (2002).